ELSEVIER

Marine Geology 163 (2000) 125–148

MARINE GEOLOGY
INTERNATIONAL JOURNAL OF MARINE GEOLOGY, GEOCHEMISTRY AND GEOPHYSICS

www.elsevier.nl/locate/margeo

Inferred gas hydrates and clay diapirs near the Storegga Slide on the southern edge of the Vøring Plateau, offshore Norway

S. Bouriak [a], M. Vanneste [b,*], A. Saoutkine [a]

[a] *UNESCO-MSU Centre for Marine Geology and Geophysics, Faculty of Geology, Moscow State University, Vorobjevy Gory, 119899 Moscow, Russian Federation*

[b] *Renard Centre of Marine Geology, Geology & Soil Sciences, University of Gent, Krijgslaan 281 S8, B-9000 Gent, Belgium*

Received 16 March 1999; accepted 24 September 1999

Abstract

This paper presents a new data set, including single-channel airgun seismic lines, OKEAN long-range side-scan sonar data and gravity cores, acquired on the edge of the Vøring Plateau and in the region of the Storrega Slide. The data acquisition was part of the 8th Training Through Research (TTR-8) expedition with R.V. *Professor Logachev*. The acoustic profiles clearly show two laterally separated zones characterised by the presence of bottom-simulating reflectors (BSRs) at about 350 ms TWT subbottom depth. The *lower BSR zone* is located on the slope of the Vøring Plateau in the immediate vicinity of the northern headwall of the Storegga Slide and, in some places, below the slide deposits. This zone runs parallel to the general trend of the continental slope. The spatial distribution of the *upper BSR zone*, located upslope in an area where diapir-like structures are found, does not demonstrate any topographic control. Interpretation of high-backscatter patches on the OKEAN sonographs associates the observed structures with fluid escape features on the seabed. Most of them are pockmarks, but in a few places, diapirs are cropping out and form dome-like elevations. After analysing the behaviour of the BSR (sometimes crosscutting) and its acoustic characteristics (reversed polarity), and after applying seismic inversion processing to estimate the acoustic velocity change across the BSR, this reflector is interpreted to represent the base of the local gas hydrate stability field (GHSF). This information was used to derive the regional geothermal gradient. Spatial variations of the inferred geothermal field appeared to be negligible. The observation of two separated BSR zones suggests different environmental controls for the growth of the hydrates. Enhanced reflectors observed in the intermediate zone can be explained by the presence of strata-bound free gas accumulations and migration combined with overlying permeability barriers. Therefore, a model for gas hydrate formation in relation to directional fluid migration processes, fluid escape features and the presence of diapiric structures is proposed in this paper. Our model is supported by sedimentological analyses of seafloor samples, which demonstrate the presence of stiff clays with evidence of gas migration, and by paleontological studies of the cores retrieved from the pockmarks. The presence of a BSR in the sedimentary section within the slide scar area implies the repositioning of hydrates to newly established equilibrium conditions after the slide event. This observation allows us to simply estimate an upper limit of the fluid migration velocity in the order of several cm/year. Finally, the effect of hydrate dissociation on slope instability is considered. Assuming that the in situ decomposition of hydrates due to instantaneous depressurisation is slow enough to permit the excess volume of released gas and water to be

* Corresponding author. Tel.: +32-9-264-45-90; fax: +32-9-264-49-67; e-mail: maarten.vanneste@rug.ac.be

0025-3227/00/$ - see front matter © 2000 Elsevier Science B.V. All rights reserved.
PII: S0025-3227(99)00115-2

re-distributed through the whole sedimentary section above the paleo-BSR (with consuming heat and increasing pore pressure, dissociation tends to shift the PT-conditions back to equilibrium values), it appears that the dissociation of hydrates due to sliding would cause only 0.2% increase of the pore pressure, which would hardly contribute to further slope instability. © 2000 Elsevier Science B.V. All rights reserved.

Keywords: gas hydrates; clay diapirs; Vøring Plateau

1. Introduction: the Storegga Slide, gas hydrates and BSRs

1.1. The Storegga Slide

The Storegga Slide situated on the passive Norwegian margin south of the Vøring Plateau is known as one of the world's biggest underwater slides. The headwall, the steepest part of the slide, is 290 km long and has an average slope gradient of 10–20°. The slide deposits are up to 450 m thick, the total run-out distance is approximately 800 km and the total displaced volume of sediments is estimated to be in the order of 5500 km^3 (Fig. 1). The slide scar area, including distal deposits, is approximately 34 000 km^2 (Bugge et al., 1987).

Based on seismic profiles, sediment samples and Gloria side-scan sonar data, Bugge et al. (1987; 1988) defined three main stages of sliding events with additional minor slides:

The first Storegga Slide occurred between 30 ka and 50 ka BP and was the largest one in terms of volume of displaced sediments. In total, about 75% of the sediments involved were deposited outside the slide scar area, i.e., below the 2700 m isobath. The first slide extends into the abyssal plain, about 350 km further downslope from the headwall. It comprises the whole slide scar area. The mobilised sediments are believed to be relatively soft, fine grained Plio-Quaternary clays. It is assumed that this mass wasting event moved in the form of a partially liquefied debris flow with enhanced pore water pressures, resulting in completely remoulded sediments (Bugge et al., 1988).

The last two major slides occurred in near succession (8–6 ka BP) and cut deeper into the more consolidated sediments in the central part of the first slide area. The deposits of the second slide are the most extensive and far-travelled: 800 km relative to the headwall in northwestern direction into the Norwegian basin. Debris flow deposits commonly occur within the area of the second slide. Furthermore, the deposits contain some large, almost undisturbed sediment units, indicating that the fluidised portion of the flow should have been relatively thick with low-permeability (Bugge et al., 1988). Probably distal deposits of this slide event are redistributed over parts of the Norwegian Sea (Bugge et al., 1987; Jansen et al., 1987).

The third event only disturbed the central and upper part of the slide scar with its headwall at 1000 m, i.e., well below that of the second slide. The deposits show an essentially blocky nature, similar to the second slide (Bugge et al., 1987, 1988).

The occurrence of gas hydrates on the Vøring Plateau and their possible relationship with the initiation of the Storegga Slide on the Norwegian shelf edge have been discussed previously (e.g., Bugge et al., 1988; Mienert et al., 1998). Bugge et al. (1987) hypothesised that the main triggering mechanism for the slides was likely to have been earthquake loading with a possible contribution of ice loading for the first slide event. The observation that inferred gas hydrates are located at the same depth as part of the gliding plane means that decomposition of hydrates may have contributed to the triggering of the slides, after an earthquake suddenly reshaped the pore pressure distribution in the sedimentary column, leading to liquefaction and weakened sediments (Bugge et al., 1987).

1.2. Gas hydrates and BSRs

Gas hydrates are ice-like mixtures of low-molecular weight gas molecules, enclosed within cages of water molecules. These structures require high pressures and low temperature conditions (e.g., Kvenvolden, 1993; Sloan, 1998). However, the main re-

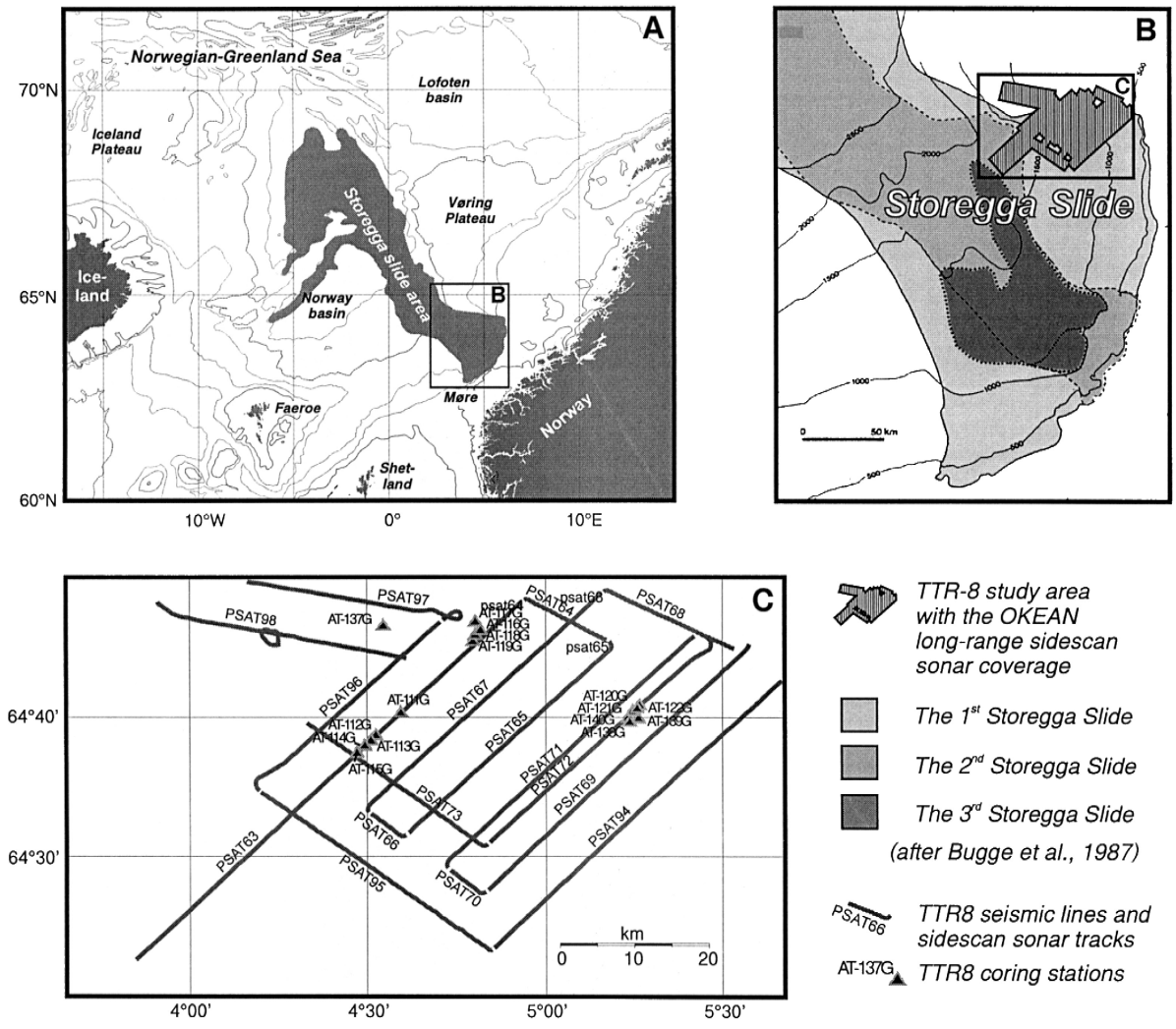


Fig. 1. Location map of the study area relative to (A) northwestern Europe and (B) the Storegga Slide (after Bugge et al., 1988), together with (C) the TTR-8 survey lines and bottom sampling stations. Seismic and OKEAN side-scan sonar data acquisition were made along the same lines.

striction for the occurrence of hydrates is the presence/supply of sufficient amounts of stabilising gas molecules (Hyndman and Davis, 1992; Rempel, 1995). Nevertheless, gas hydrates are believed to be common in continental margin areas (e.g., Mienert et al., 1998), as is confirmed by deep ocean drilling (DSDP–ODP).

Under natural conditions, the vertical extent of the gas hydrate stability field (GHSF) reaches from the seafloor to the intersection of the phase boundary with the subbottom temperature profile. The hydrates accumulate in parts of the pore spaces (typically a few percent) and in this way, their presence alters the acoustic, hydraulic and geotechnical properties of sediments (Dvorkin and Nur, 1993; Kvenvolden, 1993; Ecker et al., 1998).

On seismic records, the interface between hydrate-containing and hydrate-free sediments — which may correspond to the base of the GHSF — is often expressed as a bottom-simulating reflector (BSR). This anomalous reflector originates from the acoustic impedance contrast across an interface between

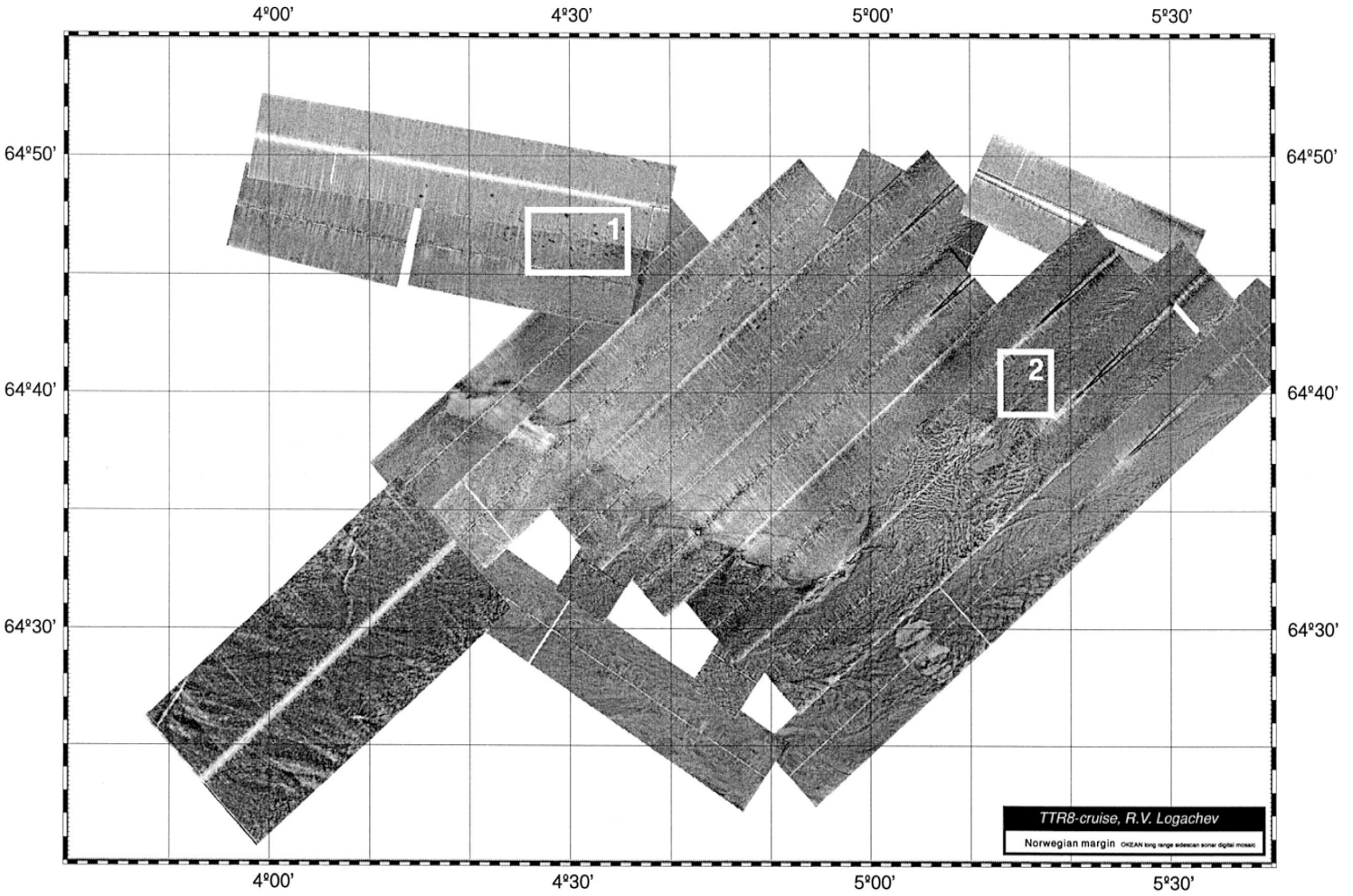


Fig. 2. Digital mosaic of the OKEAN long-range side-scan sonar imaginary. Boxes show the locations for Fig. 3.

high-velocity partially hydrate-saturated sediments above, and low-velocity probably gas-containing sediments below (Hyndman and Spence, 1992). The BSR normally mimics the seafloor topography, indicating that it is primarily temperature controlled and hence, in some regions, its presence can be used for geothermal estimations (Yamano et al., 1982). Furthermore, this high-amplitude reflector often cross-cuts the local stratigraphy and appears with negative polarity relative to the seafloor reflector (Hyndman and Spence, 1992).

1.3. Objectives of this paper

During the TTR8 cruise, carried out within the framework of the UNESCO-IOC ''Training Through Research'' (''Floating University'') Programme with R.V. *Professor Logachev*, part of the Storegga Slide area and the Vøring Plateau was investigated with a single-channel high-resolution airgun seismic reflection system, a long-range side-scan sonar and a bottom sampling programme (Fig. 1). This paper is aimed to (1) present a new multidisciplinary data set, (2) discuss the correlation between different gas and gas-hydrate related features observed, and (3) discuss their possible relevance to the submarine slide.

Analysis of the data made it possible to understand the formation mechanism of two inferred gas hydrate zones and the link with gas migration pathways, diapirs and fluid escape structures on the seafloor. Furthermore, observation of a BSR below the Storegga Slide deposits permits us to estimate the fluid migration velocity, as well as the possible contribution of gas hydrates to slope instability in the area.

2. Geological setting: Norwegian continental margin

The Norwegian-Greenland Sea is a relatively young oceanic basin, formed by seafloor spreading during the last 56 Ma. It is surrounded by passive continental margins and represents the northernmost extension of the Atlantic Ocean. The Norwegian-Greenland Sea is characterised by a peculiar hydrography of both surface (Norwegian Current, Norwegian Coastal Current) and cold dense deep or bottom (Northeast Atlantic Deep Water) water masses which are of great importance for Northern Hemisphere climate. The temperate Norwegian Current flows along the Norwegian continental margin into the Arctic ocean and plays a crucial role in the conveyor belt since the Cenozoic: its appearance and disappearance is related to the late Cenozoic glacial–interglacial cycles (Eldholm et al., 1987a; Eldholm et al., 1989a).

Based on bathymetry, morphology and structural elements, the Norwegian continental margin is subdivided into three main units: the Møre, Vøring and Lofoten-Vesterålen margin provinces (Fig. 1). The Vøring Plateau with an area of approximately 35 000 km^2 is flanked by the Lofoten basin in the North and the Norway basin in the Southwest (Eldholm et al., 1987a). It is a marginal structural high buried beneath a relatively thin veneer of Cenozoic sediments and bounded on its landward side by the Vøring Plateau Escarpment (Rabinowitz et al., 1992). Thick Cenozoic sediment accumulations characterise the area and part of the depocentre coincides with the

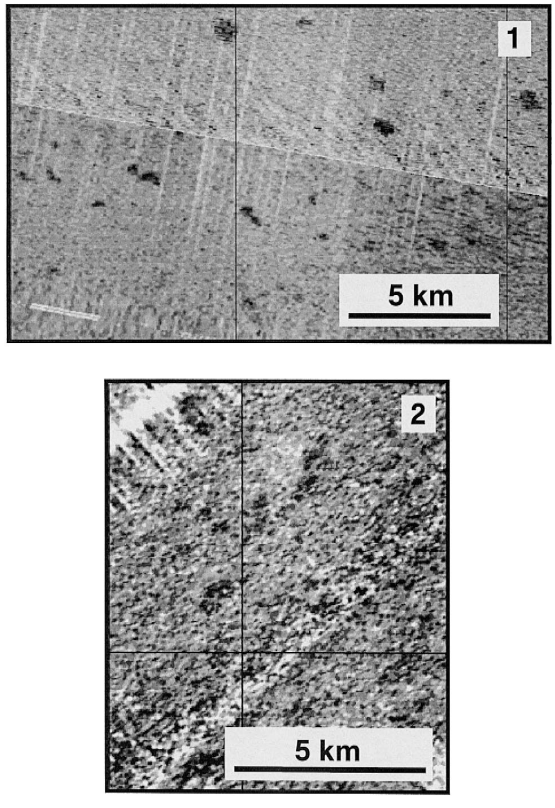


Fig. 3. Two examples of high-backscatter patches observed on the sonograph. 1 and 2 refer to the boxes in Fig. 2.

Storegga Slide area, located south of the Vøring Plateau (Jansen et al., 1987). On the marginal Vøring Plateau, diapir fields are present (Hjelstuen et al., 1997).

The potential for sediment deposition in the Norwegian-Greenland Sea responded strongly to the glacial–interglacial paleoclimatic fluctuations in the Quaternary. The regional pattern of sediment flux to the deep seafloor changed considerably (Eldholm et al., 1987a). The mainly glacial Quaternary deposits near the shelf edge in the Storegga slide area vary between 100 and over 300 m in thickness (Bugge et al., 1988).

3. Data and methods

A total of approximately 450 km of high-resolution airgun reflection seismic profiles together with OKEAN long-range side-scan sonar swath mapping of the seafloor and 15 gravity cores collected during TTR-8 expedition were examined in this study (Fig. 1).

3.1. Seismic data acquisition

The seismic system included a 2 l airgun and a single-channel hydrophone streamer with approximately 350 m offset. The data were recorded digitally (sampling interval 1 ms) within the frequency band of 50–250 Hz. The dominant frequency in water equals 180 Hz and the wavelength is 8.3 m. Only minimal processing was applied to the data to ensure a true relative amplitude recovery.

3.2. Seismic inversion procedure

A rather simple modification of a sparse-spike inversion algorithm (Russel, 1988) was applied to selected parts of the above-described seismic records. This technique and its results have previously been reported by Bouriak (1998). A reflectivity sequence is estimated for each seismic trace using an iterative procedure. Discrete reflection coefficients are added to the reflectivity sequence one by one until the error between the real trace and the synthetic trace (i.e., the convolution of the reflectivity sequence with the wavelet) is sufficiently small. The position of each reflection coefficient in the reflectivity sequence is determined by the maximum amplitude of the difference between the real trace and the synthetic one, i.e., from the position of the strongest reflection that had not yet been matched. Trial and error then yields the magnitude of each individual reflection coeffi-

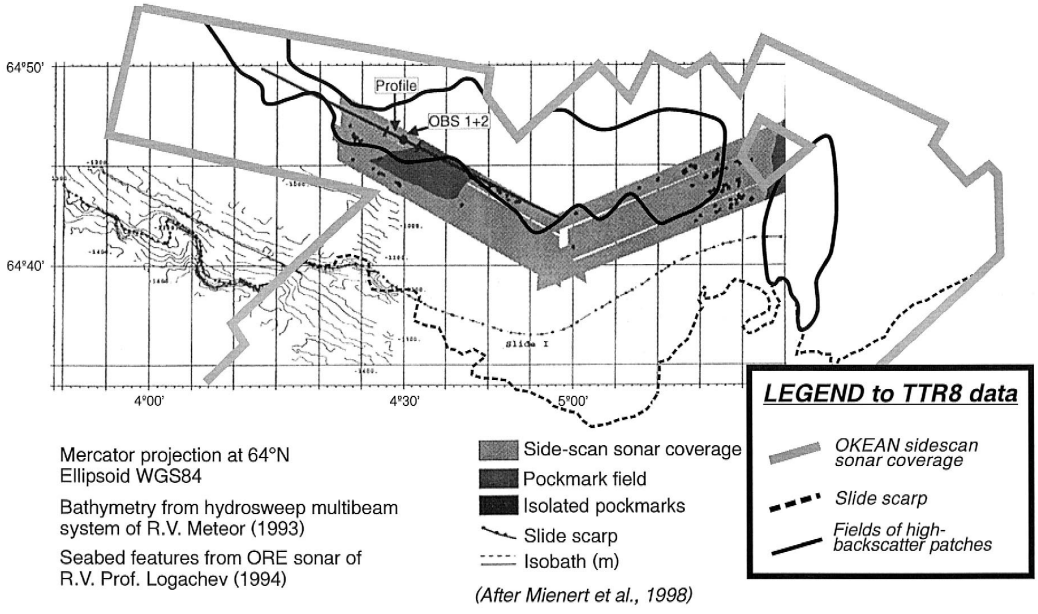


Fig. 4. Map with interpretation of side-scan sonar and hydrosweep tracks, published by Mienert et al. (1998), together with TTR-8 OKEAN mosaic interpretation. In the eastern part, the slide scarp configuration is improved using both OKEAN data and seismic data.

cient. The wavelet used for convolution is derived from the seafloor reflection for each seismic trace. The traces were reshaped to zero-phase wavelet, which allowed us to correlate the position of the individual maximum amplitudes with arrival times of different reflectors.

After proper scaling and correcting for transmission and deviation, the obtained reflectivity sequences are inverted to acoustic impedance with the recursive formula proposed by Lavergne and Willm (1977), which, in turn, was scaled into velocity with the empirical relationship between acoustic impedance and velocity proposed by Lindseth (1979). Finally, to make the result more stable and robust, the obtained ''blocky'' velocity functions were low-cut filtered to eliminate the effect of accumulation of errors, which apparently propagate through the recursive solution. As a result, this methodology only provides relative velocity information, i.e., velocity changes at major boundaries, without determining the absolute values.

3.3. Side-scan sonar survey

The OKEAN long-range side-scan sonar was operated at a frequency of 9 kHz. The swath range of the system is approximately 8 km. The OKEAN vehicle is towed at some tens of meters water depth with average speed of about 6 knots. During data processing, corrections for the varying towing speed as well as angular-variable gain were applied to compensate for spherical divergence and variations in the directional pattern of the transducers. The slant-range to ground-range corrected data were finally geographically adjusted to obtain a digital mosaic (see also Akentieva and Shashkin, 1998). The seismic and side-scan sonar data were collected simultaneously along the same lines.

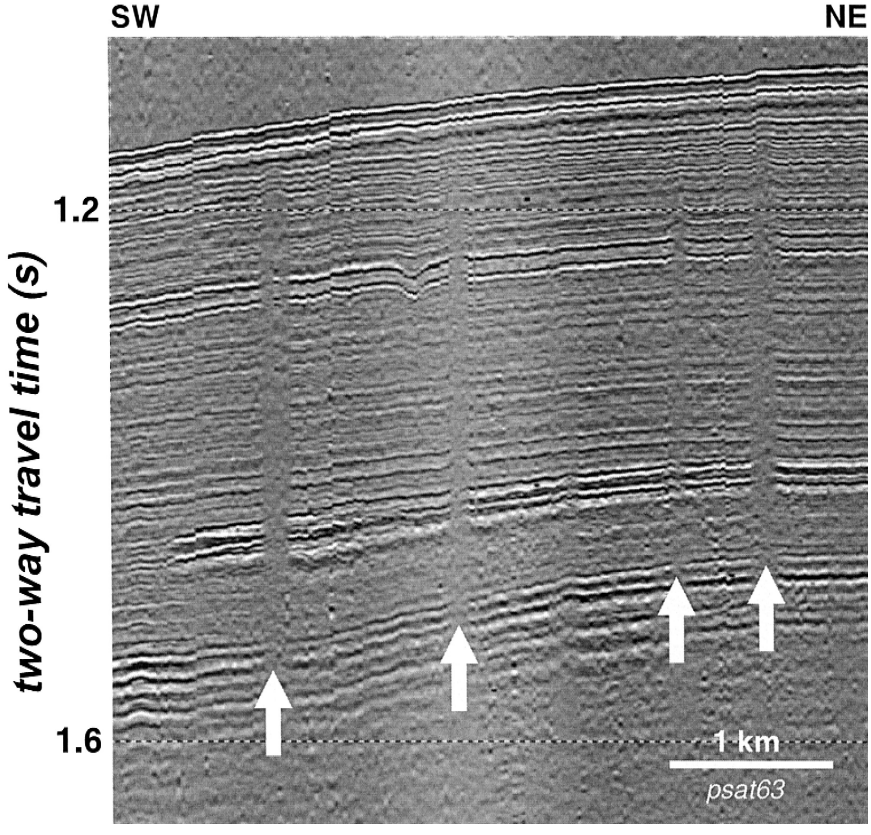


Fig. 5. Airgun seismic profile (PSAT63) showing vertical zones of acoustic wipe-outs (diapirs?) on the upper slope of the Vøring Plateau.

3.4. Sampling programme

The seafloor-sampling programme was carried out with a gravity corer (6.6 m long, 168 mm diameter, 1500 kg weight) with an inner plastic liner that allowed the collection of up to 6 m of undisturbed sediments. The ship positioning was obtained with a GPS navigation system and the locations of the coring stations relative to the features of the seafloor relief were also checked with a low-frequency (6 kHz) echosounder, which was active during all coring operations. In this work, we use visual lithological core descriptions made on board, plus micropalaeontological studies of calcareous nannofossils (coccoliths) examined in smear-slides using Olympus Light Microscope with magnification of 1000 ×. Unbroken coccoliths were identified using the system of Cenozoic calcareous nannofossils published by Bolli et al. (1985). In case of poor preservations and impossibility of precise identification of species, open nomenclature was used.

4. Observations and results

4.1. Seafloor fluid escape structures and clay diapirs

The deposits of the first Storegga Slide event and its escarpment can be clearly seen on the digital mosaic of the side-scan sonar imaginary (Fig. 2). North of the escarpment, on the upper part of the Vøring Plateau slope, numerous patches of higher backscattering were observed (Fig. 3). Their distribution fits the pockmark fields reported by Mienert et al. (1998), with allowance made for differences in operating frequencies, resolution and penetration of the high-resolution deep-towed instrument, used for that study, and the OKEAN system (Fig. 4). More specific, many of the structures observed by the high-resolution instrument are probably too small to be resolved on the OKEAN sonograph. On the other hand, the greater penetration depth of the OKEAN system allows us to observe some buried features that cannot be seen on the high-resolution data. The

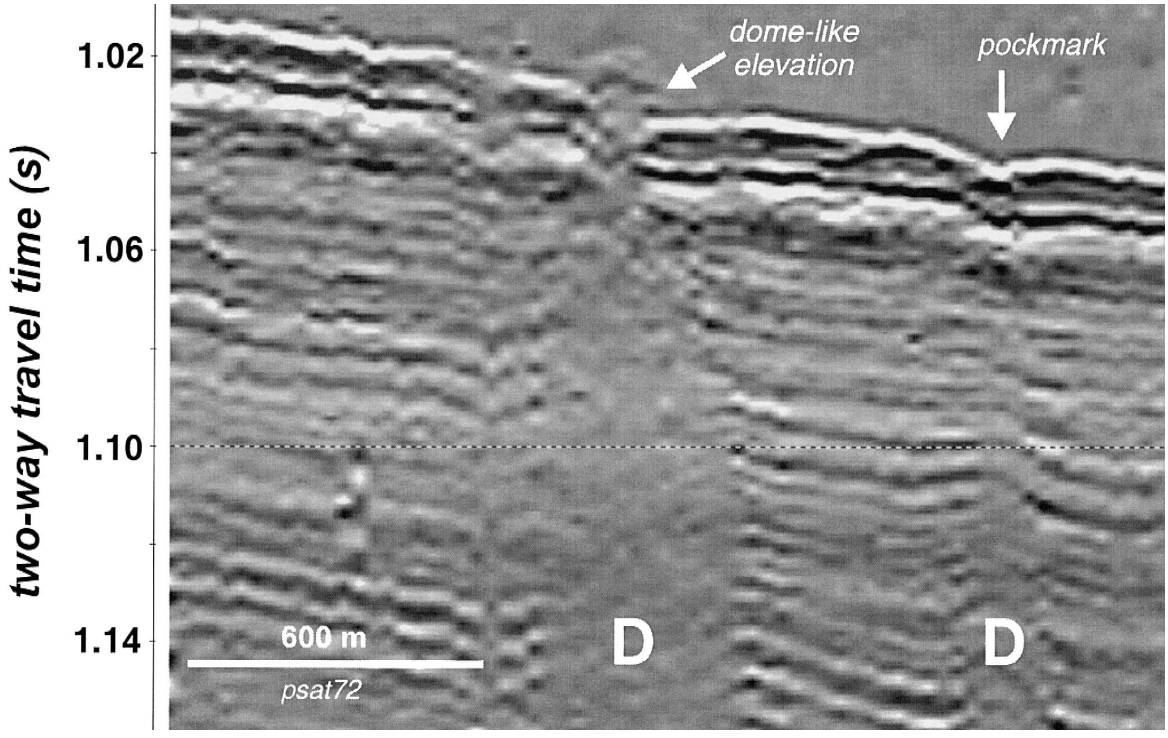


Fig. 6. Wipe-out zones (''D'') cropping out: a dome like elevation and a pockmark on the seafloor as observed on the seismic record along line PSAT72. Note the slightly up-pulling marginal reflections.

difference in operating frequencies of the two side-scan sonar sources also suggests different dimensions of scattering elements at the seafloor and in the sub-seafloor sediments, which would affect the resulting imagery most efficiently. The lower resolution and shallower towing depth of the OKEAN system does not allow us to explain the observed patches simply by seafloor topography but suggest the enhanced backscatter as being caused by local changes of the physical properties of the seafloor and sub-seafloor sediments. This can be confirmed by the presence of gas-charged sediments and carbonate crusts in all cores taken from the patches (AT-117G, 118G, 120G, 121G, 122G, 139G, and 140G).

Seismic airgun records along the same part of the slope are characterised by narrow (150–500 m in width) vertical zones of acoustic wipe-outs (Fig. 5). In vertical dimension, the ''wipe-out zones'' are traced typically for around 300 m (400 ms TWT), with their base below the penetration depth of the seismic system. Similar acoustic features were previously reported in this area by Baas et al. (1994) and Evans et al. (1996), who believed that these anomalies are caused by vertical fluid (gas?) expulsion. In two places, we noticed that these features are cropping out at the seafloor, forming dome-like elevations similar to small-scale (up to 7 m high) mud volcanic structures. In other cases, the ''wipe-out zones'' approach the seafloor and are often accompanied by small pockmarks. In deeper parts of the sedimentary section, these features are frequently characterised by up-pulling of marginal reflectors, rather suggesting vertical sediment movement than pure fluid migration processes (Fig. 6).

Nannoplankton Zones and Stratgraphic Intervals Used in the Norwegian-Greenland Sea (DSDP, Leg 38) (after Muller, 1976)

Age	Nannoplankton Zonation	Species
Quaternary	*Emiliania huxleyi*	*Coccolithus pelagicus, Cyclococcolithus leptoporus, Discolithin japonica, Emiliania huxleyi, Gephyrocapsa ericsonii, Syracosphaera pulchra*
	Gephyrocapsa oceanica	*Coccolithus pelagicus, Cyclococcolithus leptoporus, Gephyrocapsa ericsonii, Helicosphaera carterti, Syracosphaera pulchra*
Late Pliocene	*Pseudoemiliani huxleyi*	*Coccolithus pelagicus, Cyclococcolithus leptoporus, Gephyrocapsa ericsonii, Gephyrocapsa sp., Helicosphaera carterti, Helicosphaera sellii,Syracosphaera pulchra*
Early Pliocene Middle Miocene	*Reticulofenestra pseudoumbillica*	*Coccolithus pelagicus, Discolithin japonica,* ***Reticulofenestra pseudoumbilica****, Sphenolithus abies*
Early Miocene	*Helicosphaera ampliaera*	*Coccolithus pelagicus, Helicosphaera ampliaperta,* ***Reticulofenestra cf. pseudoumbilica***
	?	same species as in the *Spenolithus distentus* zone plus *Discolithina enormis*
Late Oligocene	*Sphenolithus ciperoensis*	
Middle Oligocene	*Sphenolithus distentus*	***Chiasmolithus altus,*** *Coccolithus abisectus, Cocoolithus pelagicus,* ***Cyclococcolithus floridanus, Dictycococcites dictyodus,*** *Discoaster deflandri, Sicolithina desueta, Helicosphaera euphratis, Helicosphaera perch-nielsenae,* ***Helicosphaera recta,*** *Reticulofenestra elatrata, Reticulofenestra lockeri, Sphenolithus moriformis, Zygrhablitus bijugatus*
Middle Oligocene	?	***Chiasmolithus oamaruensis, Cribocentrum reticulatum, Cyclococcolithus luminis,*** *Discolithina pulcheroides, Isthmolithus recurvus,* ***Reticulofenestra umbilica,*** *Transversopontis obliquipons*
Early Oligocene Late Eocene	*Isthmolithus recurvus*	
Late Eocene Middle Eocene	*Reticulofenestra umbilica*	***Braarudosphaera bigelow, Reticulofenestra umbilica, Zygolithus dublus***
Early Eocene	?	***Braarudosphaera bigelow,*** *Chiasmolithus solithus,* ***Cyclococcolithus luminis, Discoaster lodensis,*** *Discoasteroides kuepperi, Discolithina pulchra, Imperiaster obscurus, Marthasterites tribrachiatus, Micrantholithus mirabilis, Zygolithus dublus*
	Imperiaster obscurus	

bold: coccoliths found in some diapirs out-crops and pockmarks during TTR8 Leg 3.

Coccoliths founds in the TTR8 cores

Cores from diapir out-crops and pockmarks	Backgrounds cores from surroundings
AT117G *M. staurophora* (148 cm from the top) ***Chiasmolithus oamaruensis Cribocentrum cf. reticulatum, Cyclococcolithus luminis, R. umbilica, Braarudidosphaera bigelow, Discoaster lodoensis*** (394 cm from the top).	**AT111G** *Micula staurophora* (134 cm from the top)
AT118G *M. staurophora* (47 cm from the top) ***Ch. oamaruensis,Cr.cf. reticulatum, Ch. altus, Helicoshpaera recta, Zigodiscus cf. dubius*** (92 cm from the top).	**AT112G** *M. staurophora* (26 cm from the top)
AT120G *M. staurophora,* (138 cm from the top)	**AT113G** *M. staurophora* (211 cm and 417 cm from the top)
AT121G *Biantolithus cf sparsus, M. staurophora,* ***R. pseudoumbilica, Dictycoccites cf. dictyodus.***	**AT114G** *M. staurophora, Reticulofenestra cf. umbilica, Discoaster sp* (357 cm from the top)
AT122G *M. staurophora*	**AT115G** *M. staurophora* (10 cm), *Chiastozigus litterarius* (259 cm from the top)
AT139G *M. staurophora,****B bigelow, Cr. cf. reticulatum*** (93 cm from the top)	**AT116G** *M. staurophora, Cribosphaerella sp* (336 cm from the top)
AT140G ***Ch. oamaruensis, Cyclococcolithus floridanus, R. umbilica,*** *Reticulofenestra sp.* (244 cm from the top)	**AT119G** *B. bigelow, R. pseudoumbilica, Cribocentrum sp ? (162 cm from the top) M. cf. staurophora (240 cm from the top)*
	AT138G *M. staurophora, R. pseudoumbilica* (20 cm from the top).

bold: coccoliths described in sites from Norwgian-Greenland Sea (DSDP, Leg 38)

Fig. 7. Nannoplankton zones and stratigraphic intervals used in the Norwegian-Greenland Sea (DSDP, Leg 38) (after Muller, 1978) and the pre-Quaternary nannofossils found in the TTR-8 cores.

These indirect acoustic evidences of mass transport phenomena are confirmed by analysing the core samples. Cores AT-120 and AT-121 are taken from one of the dome-like seabed elevations. The recovered sediments are mainly composed of stiff homogeneous and gas-saturated clays, which were much more consolidated than recent hemipelagic sediments. Paleontological studies of the sampled cores are summarised in Fig. 7. These studies revealed that, beside Quaternary fossils and ice-rafted debris fossils found in all the cores, the sediments taken from the dome-like elevation and pockmarks contain Tertiary fossils, mainly of Eocene to Oligocene age. In our opinion, these fossils can hardly be transported over several hundreds of meters only by fluid migration. Therefore, the observed vertical ''wipe-out zones'' should most likely be considered not as pure gas-related acoustic features, but as clay diapirs originating from formations of Tertiary (probably Eocene) age.

4.2. Seismic evidence for gas hydrates and shallow gas and implications for determining the geothermal regime

The single-channel airgun reflection seismic data collected during the TTR-8 cruise show a distinct bottom-simulating reflector at subbottom depths of approximately 350 ms TWT, as well as enhanced reflections (bright spots) indicating shallow gas accumulations. Fig. 8 shows part of a time-section along line PSAT63, on which these features — typical of the whole area — are most prominent. The high-amplitude BSR, terminating just landward of the slide scarp, mimics the seafloor topography, clearly crosscuts the local stratigraphy and appears

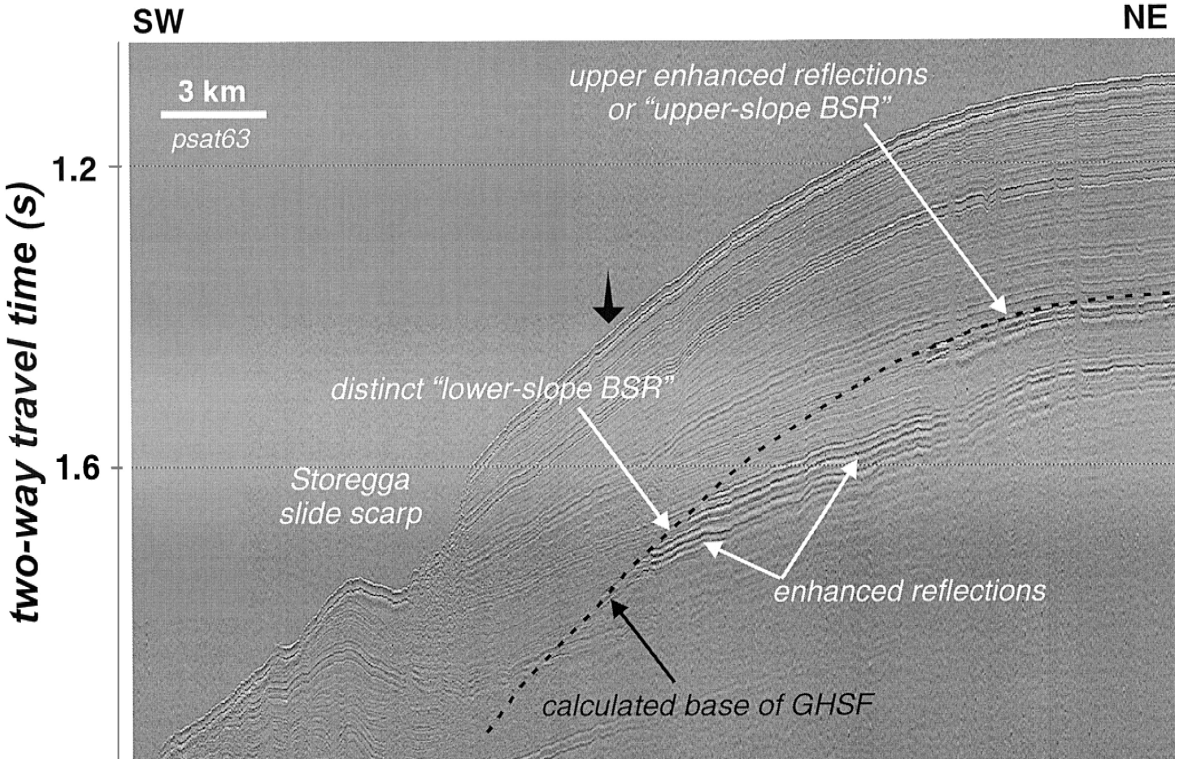


Fig. 8. Part of time-section along line PSAT63 with a clear BSR and enhanced reflections. The black dashed line respresents the calculated base of the GHSF along this line. Since the difference between the hydrostatic pressure approach (geothermal gradient of 0.0515°C/m) and lithostatic approach (geothermal gradient of 0.0558°C/m, average bulk density 1800 kg/m^3) is very small, only the lithostatic one is shown. Note that the upper enhanced reflection fits well to the GHSF base and thus is likely to be also gas hydrate related. The black arrow indicated the reference point used for geothermal calculations, and at the same time the location of the seismic traces shown in Fig. 9.

with reversed polarity relative to the seafloor reflection (Fig. 9). Slope upward in NE direction, packages of enhanced reflectors are observed. However these bright spots fade out in the diapir field further upslope.

The ''upper'' enhanced reflector on Fig. 8 also closely follows the seafloor morphology. It is seen on the upper slope at nearly the same subbottom depth as the above mentioned BSR. At first instance, this particular reflector was not considered as being linked with gas hydrates because no clear crosscutting was observed due to a sedimentation pattern that parallels the seafloor as well, although polarity analysis showed phase reversal, similar to the situation presented in Fig. 9.

BSRs were observed on all lines perpendicular to the slope in the undisturbed sediments of the Vøring Plateau, and on the three easternmost lines below the Storegga Slide deposits. Fig. 10 shows perhaps the most interesting example of the BSR observation in the area. Here, the reflector starts directly below the slide scarp and continues SW inside the slide area, simulating the present-day seafloor topography. An enhanced reflector is also seen to the NE of this BSR.

In order to derive or model the geothermal regime from the presence of BSRs on seismic records, some aspects and assumptions had to be taken into account. These are mainly based on literature study and the results published from ODP leg 104, sites 642 (67°13.5′N, 2°55.7′E), 643 (67°42.9′N, 1°02.0′E) and 644 (66°40.7′N, 4°34.6′E) located on the Vøring Plateau at 250–400 km to the N–NW of the study area (Eldholm et al., 1987b; Eldholm et al., 1989b). More details and formulas are given in Appendix A.

First of all, the BSR is assumed to correspond to the base of the GHSF and hence its subbottom position is supposed to coincide with the bulk thermodynamic 3-phase equilibrium boundary of the gas–seawater–hydrate mixture. The influence of the pore size distribution (capillary effects) throughout the GHSF and surface properties (activity) of the host material on hydrate stability is ignored. Including these effects should result in lower subbottom depths of hydrate stability (Clennell et al., 1999).

Although no hydrates have been recovered in this area, we assume a pure methane–seawater–hydrate mixture to be present since methane is by far the most abundant hydrate forming gas in nature (Kvenvolden, 1998). In contrast to the low gas content in sediments of the outer Vøring Plateau (sites 642, 643), analysis at site 644 on the inner Vøring Plateau demonstrated that the present gas is mainly isotopically light methane (> 99.9%), suggesting a biogenic origin (Kvenvolden et al., 1989).

Since the seismic data were acquired in single-channel form, no absolute velocity analysis can be performed. For estimating the subbottom position of

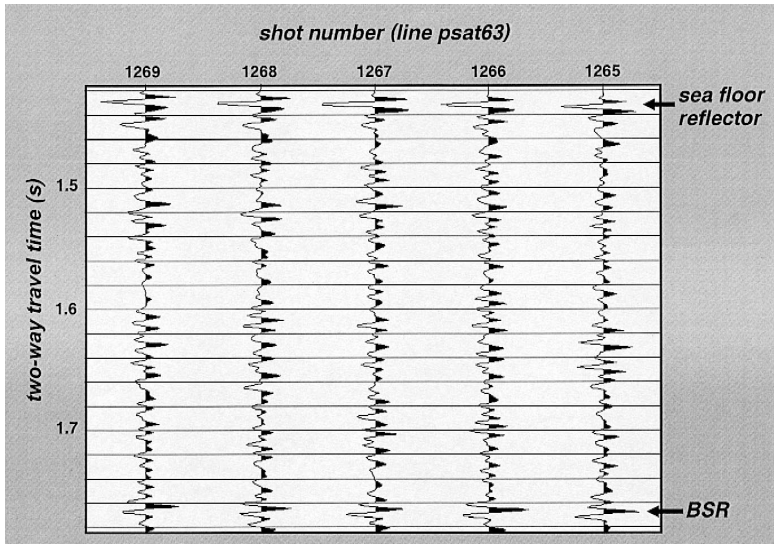


Fig. 9. Seafloor reflection and the BSR signature with reversed polarity, taken from line psat63.

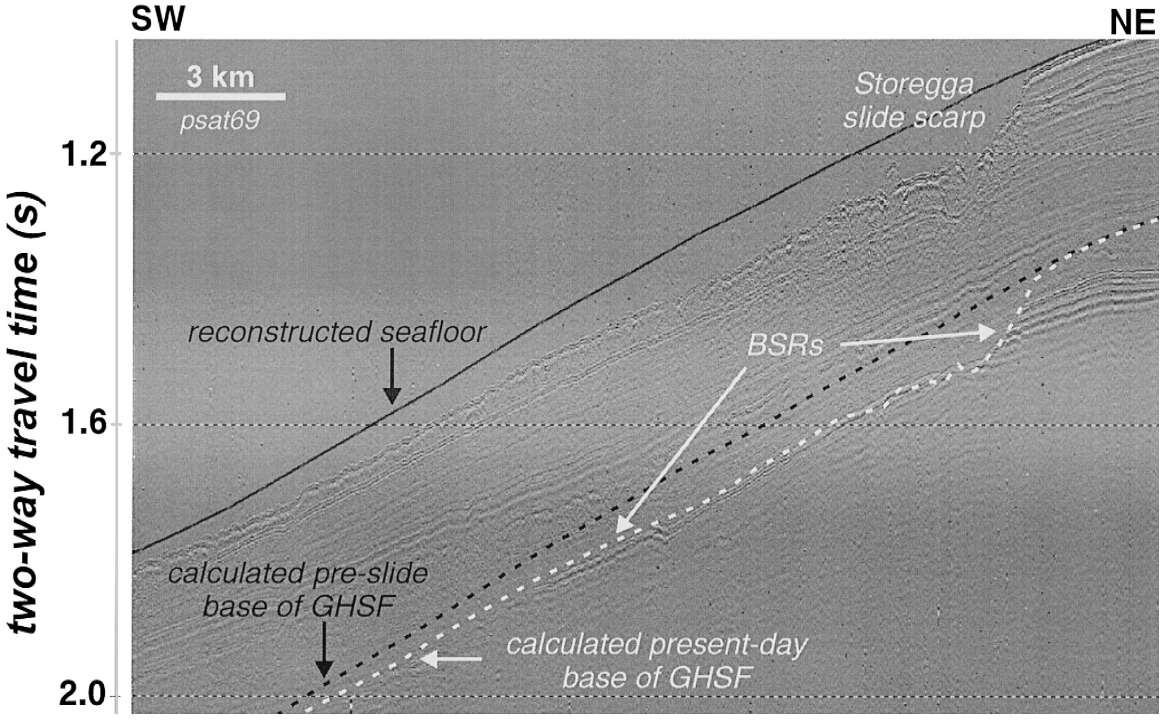


Fig. 10. Part of the seismic profile PSAT69, demonstrating a BSR below the slide scarp and deposits of the 1st Storegga Slide. Also the reconstruction of the paleo-seafloor topography along this line PSAT69, together with the calculated depths of the base of the GHSF for the present-day situation and in pre-slide seafloor conditions are shown. The intermediate position of the base of the GHSF, i.e., immediately after the slide, is not indicated since the vertical shrinking is only in the order of a few meters and hence cannot be resolved on this scale.

the BSR, an average regression equation relating the mean compressional wave velocity to subbottom depths and later to two-way travel time was determined. This equation is obtained using the p-wave velocity measurements (combined) in ODP site 642 and 643 (Eldholm et al., 1987b). Furthermore, the results are compared with the more general regression equation of Hamilton for terrigeneous sediments (Hamilton, 1980) like silt clays, turbidites and mudstone shale.

The bottom water temperature in this area is taken to be 0°C, consistent with values mentioned in Mienert et al. (1998) (''around 0 to -1°C on the mid-Norwegian slope and within the pockmark field'') and Thiede et al. (1989) (''<0–1°C below 500 m isobath in the Eastern Norwegian Sea'').

The subbottom temperature profile was assumed to be linear with increasing depth, i.e., a steady-state situation in the sedimentary section above the base of the GHSF. Diverse factors altering the temperature gradient and thus the vertical extent of the GHSF (e.g., subsidence, compaction and continuous sedimentation, changes in bottom water temperature, sea level changes, ...) are disregarded.

Since we do not have access to accurate pore pressure profiles as a function of subbottom depth, the geothermal field and its lateral variability are investigated for both end members, i.e., the hydrostatic pore pressure distribution and the lithostatic alternative. For calculations of the lithostatic pressure, porosity changes vs. depth above the BSR were ignored and an averaged maximum saturated bulk density of 1.8 g/cm^3 was used, based on the data of ODP Leg 104 hole 644 (Eldholm et al., 1987b).

A first estimate was performed using a single BSR point on profile PSAT63, indicated on Fig. 8. The thermal gradient was found to equal 0.0515°C/m (assuming hydrostatic pore pressure distribution) or

0.0558°C/m (assuming lithostatic pore pressure). Results obtained using Hamilton's regression curve were almost identical: the calculated differences appeared to be less than 5%. Similar values for the geothermal gradient were reported by Mienert et al. (1998). These calculations — in turn — were used to delineate the theoretical GHSF in the area, for example on line PSAT63 (Fig. 8). The difference between the two approaches mentioned cannot be resolved on the seismic line, and hence, only the results of the lithostatic pressure method is shown. In either case, spatial fluctuations of the gradient within the area are negligible, as on all of the acoustic profiles the BSRs were observed at depths close to the theoretical GHSF limit.

Remarkably, the ''upper'' enhanced reflections, where these exist, also fit the same calculated lower limit of the GHSF (Fig. 8) and thus are most likely

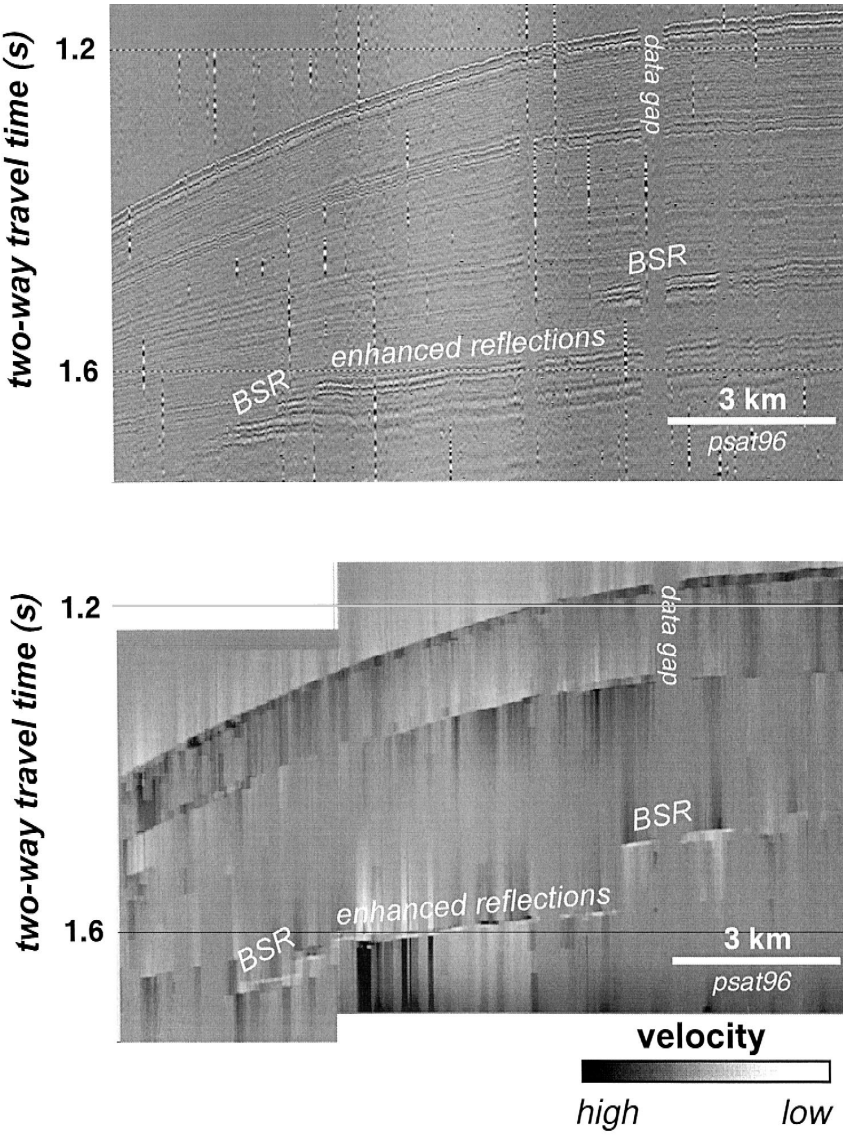


Fig. 11. Airgun profile PSAT96 with BSRs and enhanced reflections (above), and a relative velocity model derived from seismic inversion applied to the same seismic section (below).

of similar nature and should be referred to as gas hydrate BSRs too. On this figure, it is clear that both BSR occurrences coincide very well with the theoretical GHSF, while the enhanced reflectors in the intermediate zone lie below the GHSF.

The results of the seismic inversion procedure corroborate the reliability of inferring gas hydrates in two separated zones and free gas accumulations in the intermediate area for explaining the seismic observations. Both BSR events and the long continuous enhanced reflections in between of the two hydrate zones correspond to boundaries where the acoustic compressional wave velocity decreases substantially (Fig. 11). A relative velocity drop of approximately 350 m/s was found to be present at both BSR occurrences. Partial hydrate occupations of the pore spaces above the BSRs and probably some percentage of free gas below form a plausible explanation. Unfortunately, the inversion results do not allow us to estimate the total fraction of hydrates in the pore spaces and/or the volume of free gas under the GHSF. In the intermediate section, the sudden velocity drop near the enhanced reflectors seems to have a smaller magnitude, due to the lack of hydrates. However, the complex acoustic interference pattern in this area complicates the analysis and prognosis.

In the northern rim of the Storegga Slide, a high-amplitude reflector with phase reversal at approximately 375 ms TWT subbottom depth was also observed on airgun data by Mienert et al. (1998). Using high-frequency OBS measuring tools, Posewang and Mienert (1996) found a sudden velocity decrease from ± 1900 m/s to values between 1300 and 1400 m/s, pointing towards the presence of free gases in a zone of 10 to 30 m under the GHSF. This confirms the results obtained with our velocity inversion.

In all cases, the BSR represents a sharp interface at the source frequency used while no reflection of the top of the hydrate layer is observed. Posewang

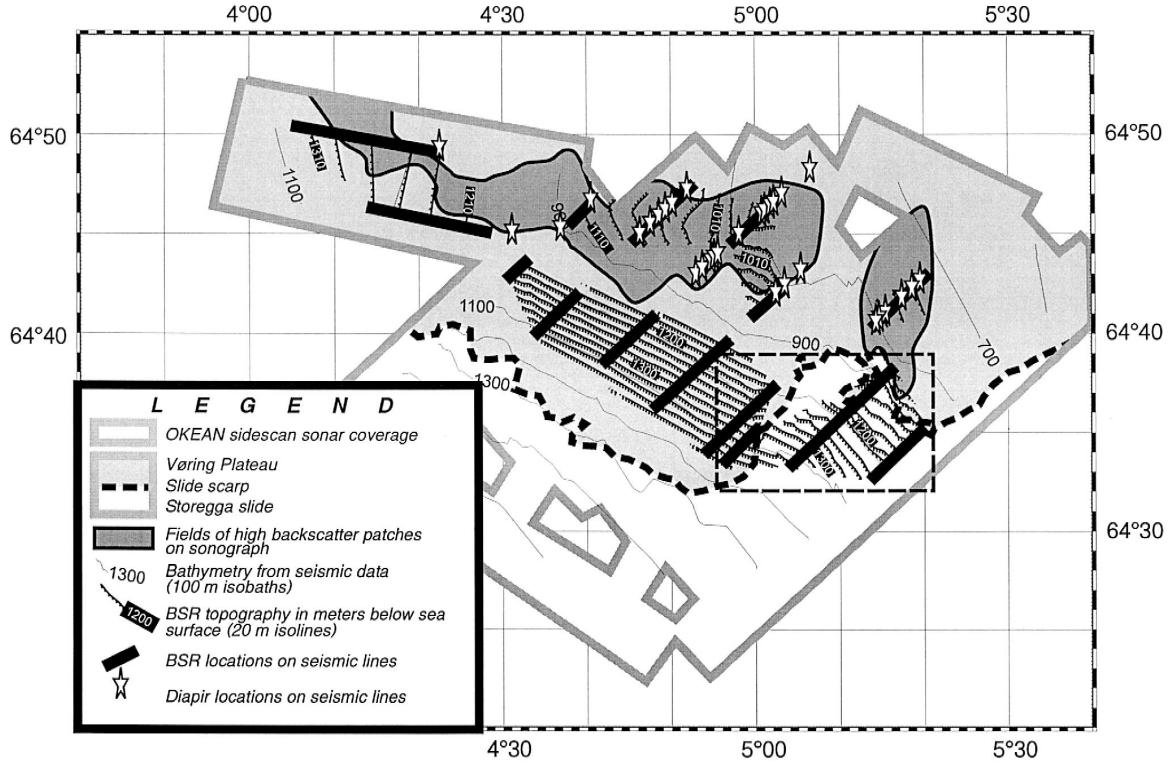


Fig. 12. Observations and interpretation of the TTR8 OKEAN long-range side-scan sonar mosaic and airgun seismic profiles. Note two separate zones of BSR distribution and the presence of BSRs in the slide area. Box shows location of Fig. 15.

and Mienert (1996) and Mienert et al. (1998) reported for the first time the occurrence of a double BSR event on one and the same acoustic cross-section in the same area. This feature is however not observed on our seismic records.

4.3. Link between inferred hydrates and fluid escape features

Fig. 12 summarises and combines all the above-described observations, showing the typical seafloor expressions and the different features observed on the seismic data.

The BSR occurrences in the study area appear to form two separated zones. One elongated zone (''lower-slope BSR'') is traced along the lower slope of the plateau and runs virtually parallel to the general trend of the slope. No fluid escape features were observed on the seafloor in this part of the area. In the southeastern part of the area within a territory of about 100 km^2, this ''lower slope BSR'' is also observed below the slide scarp and below the sediments mobilised during probably the first sliding event.

Another zone is located up slope, and is therefore referred to as ''upper-slope BSR'' zone. This zone does not demonstrate any morphological controls but fits nicely to the areas of interpreted fluid escape features observed on the OKEAN sonographs, in relation to the core analyses (see also 4.1). The diapirs, visualised on the seismic records, also seem to be related to the same areas, suggesting a close link between all these phenomena.

5. Discussion

5.1. Nature of the BSRs

In recent years, some models have been proposed to account for gas hydrate formation and accumulation and the development of BSRs in oceanic settings (Kvenvolden, 1998). In the first model, methane is assumed to be generated microbially in situ from organic matter (Claypool and Kaplan, 1974) and gas hydrate formation takes place concurrent with sedimentation. In the second model (Hyndman and Davis, 1992), gas hydrates are formed by removal of dissolved methane of biogenic or thermogenic origin derived from upwelling pore fluids as they enter the GHSF. In a third model (Minshull et al., 1994), free gas is supposed to migrate upwards through zones of higher permeability due to buoyancy, capillary forces and overpressuring mechanisms. Hydrates start to form at nucleation or growth sites and can form a seal, trapping free gas under the hydrate accumulations. As mentioned by Ginsburg and Soloviev (1997), active fluid migration can be either diffusive (percolation) or focused.

The distribution of the BSRs in this part of the Norwegian continental margin in two localised but separated zones with — most probably — different factors controlling their shape and spatial distribution contradicts the first model. In case of in situ methane formation, one would expect the zonality to be less striking, and the area of BSR distribution probably more regional and less organised. Furthermore, it is doubtful in general whether the microbial productivity and the amount of organic matter in sediments are high enough to provide sufficient amounts of methane for gas hydrate formation and accumulation (Hyndman and Davis, 1992).

The second model seems to fit better the observations. However, focused fluid flow can probably be ruled out, since there is an obvious lack of noticeable variations in the temperature gradient calculated from the BSR depths and the morphology of the BSR reflector. This suggests that the temperature profiles everywhere in the area are mainly conductive and advection of heat, normally associated with focused upward fluid fluxes, is negligible.

Therefore, we propose the following combined model of hydrate formation in this area, taking into consideration all the above mentioned observations and models. Our model, presented in Fig. 13, suggests active vertical percolation of methane in the zone of the ''lower-slope BSR''. Once the fluids enter the GHSF, the gas molecules are captured into hydrate structures, according to the model of Hyndman and Davis (1992). The effective porosity decreases due to the fractional filling of the pore spaces with hydrates, and hence, the permeability also drops, leading to a trap under which free gas can accumulate (Ecker et al., 1998). In the intermediate area between the ''lower-slope BSR'' zone and ''upper-slope BSR'' zone, a less permeable stratigraphic

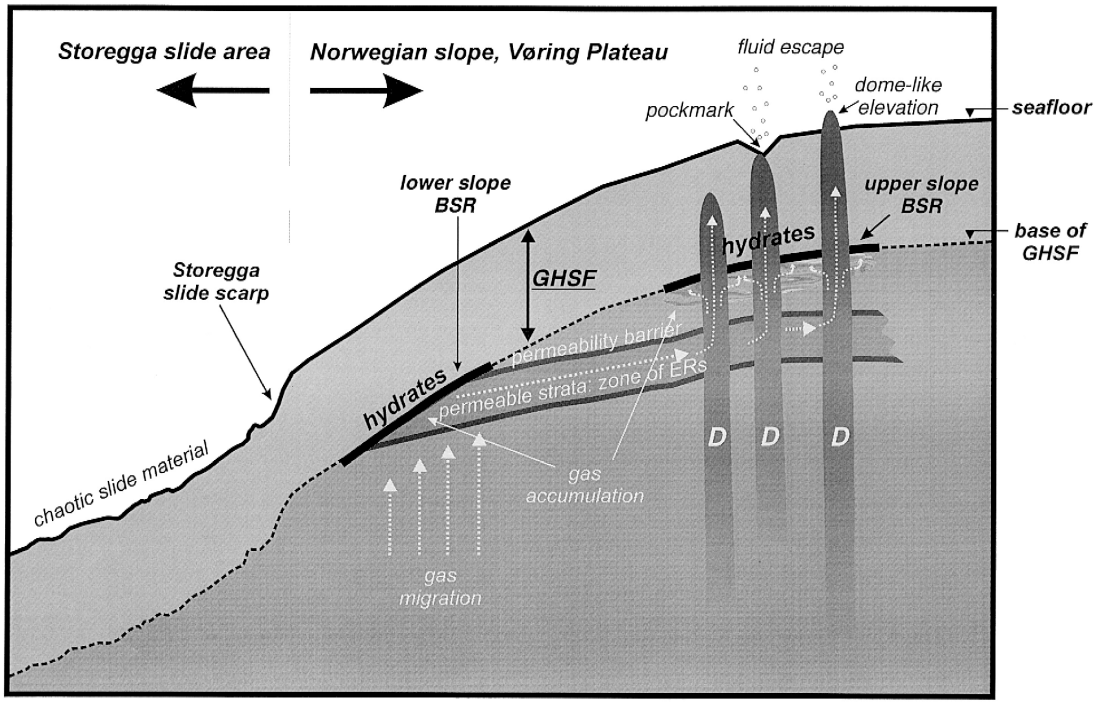


Fig. 13. A schematic model of the BSR development in the area and their link to probable clay diapirs and fluid escape features observed on the seafloor (ERs = Enhanced Reflectors).

boundary is assumed to be present below the GHSF but overlaying the enhanced reflectors, allowing free gases to accumulate or to migrate laterally towards the area characterised by the diapirs. The diapiric structures, in turn, provide possible migration pathways for further upward fluid transport to the base of the GHSF, where again hydrates can start to fill the pore spaces and thus the upper-slope diapir-related BSR formation takes place. The remaining gas, not clathrated into the hydrate structure (Clennell et al., 1999), exhausts at the seafloor creating the observed fluid escape features (pockmarks and small mud volcanoes) (Hovland and Judd, 1988), as observed on the sonographs as patches of higher backscattering.

5.2. Fluid migration velocity estimation

Based on the fact that the BSR — when observed in the sedimentary section just below the slide scarp and displaced sediments — mimics the present-day seafloor topography and, thus, appears to have already repositioned itself to the new hydrate pressure-temperature equilibrium conditions after the sliding event, it is possible to make a crude estimation of the vertical fluid migration velocity in the area of the ‘‘lower-slope BSR’’.

Using mass, momentum and energy conservation equations, it has been calculated that for a fluid velocity of 1 mm/year, the rate of hydrate formation and accumulation due to advection of methane from depth filling 1% of pore volume is of the order of 100 000 years (Rempel and Buffett, 1998; Zatsepina and Buffett, 1998). Here, we assume that a filling of 5 to 10% of the pore volume with gas hydrates is sufficient to explain the observed BSR reflection and related relative compressional wave velocity drop. Taking into account the dating of the first Storegga Slide event as 30–50 ka BP (Bugge et al., 1988), we can speculate that the subbottom fluid migration velocity in this area is of the order of at least several centimetres per year. Since, as discussed above, the conductive heat transport in the area is supposed to be by far more important than advective heat trans-

fer, this estimated quantity also represents in our opinion an upper limit for the fluid displacement rate.

5.3. Relevance of gas hydrate dissociation to further slope instability

The possible influences of sliding, and in particular the Storegga Slide events, on gas hydrate destabilisation and related liquefaction and vice versa has been actively discussed. For instance, Bugge et al. (1987) and Jansen et al. (1987) proposed gas hydrate decomposition due to earthquake agitation of sediments as one of the most likely triggering mechanisms for the Storegga Slide. Mienert et al. (1998) noticed that, as a consequence of earthquakes or mass wasting events which provoke gas hydrate to decompose due to changing thermodynamical conditions, the release of huge amounts of free gases and water in the pore space would exceed by far the volume that was previously occupied by the solid gas hydrate structure. This process can lead to — eventually drastically — increased pore pressures, facilitating further sliding. Next to that, the rapid release of methane during major slide events in coincidence with gas hydrate dissociation might have serious implications for the marine methane cycle and possibly for the global climate system (Lammers et al., 1995). Thus, any quantitative estimates of these effects are of significant interest.

The observation of BSRs inside the slide scar area and below slide deposits makes it possible to estimate how sliding could affect the gas hydrate stability in this area. It should be emphasised that such a procedure strongly depends on the assumptions made about the pore pressure distribution. In case of hydrostatic pore pressure distribution, no sliding nor earthquake would affect the overall hydrate stability.

After removal of the uppermost sediment of the seafloor, the hydrostatic pore pressure would remain unchanged since this value is only dependent on the height of the entire overlying water column.

At the same time, the seafloor is now formed by sediments initially exposed at higher temperatures due to burial under the suddenly removed sediments. The temperature difference between the seabed and the bottom water mass will cause a gradual decrease of the temperature of the ''new'' seafloor and subbottom sediments. As a consequence, the base of the GHSF will slowly move deeper into the sediments, until a new equilibrium position is reached.

This means that sliding or earthquake triggering can only force the solid hydrate structure to dissociate if excess pore pressures are present and the induced sediment failure would lead to a decrease in pore pressure. After the slide event, the theoretical base of the GHSF will then first jump immediately to a shallower subbottom depth, and only afterwards will start gradually to move deeper following the temperature decrease to the new equilibrium position (Fig. 14).

For the area of about 100 km^2 where the BSRs occur within the slide area, we have reconstructed the paleo-seafloor (i.e., the situation before the first Storegga Slide event) and calculated the position of the base of the GHSF before sliding. Fig. 10 shows an example of this reconstruction along seismic profile PSAT69. The sudden removal of the uppermost sediments caused an instantaneous decrease in lithostatic pressure (< 0.5 MPa) in the sediment column, while the in situ temperature regime at the same time is not altered. This means that the hydrates at the base of the initial stability field will fall out of the newly established pressure-induced stability field, just after the first Storegga slide event, similar as what is presented in Fig. 14. The position of the base of the GHSF immediately after the slide was then calculated, simply using the ''post-slide'' lithostatic pressure distribution and the ''pre-slide'' in situ temperature and geothermal gradient, in combination

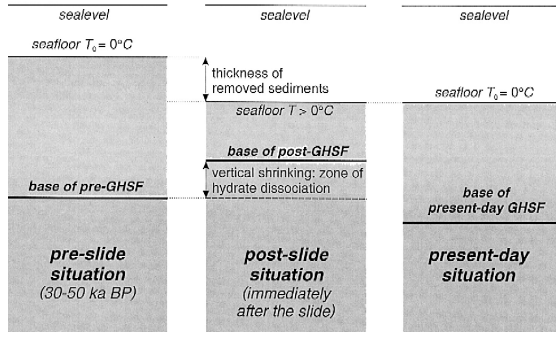


Fig. 14. Sketch of the influence of the slide event on the subbottom position of the base of the GHSF. The pre-, post and present-day situations of the vertical extent of the GHSF are shown.

with the formulas mentioned in Appendix A. A triangulation contour map of the vertical shrinking of the GHSF in this area, i.e. the thickness of that part of the initial ''pre-slide'' GHSF falling out of the ''post-slide'' GHSF, is shown in Fig. 15. The use of a lithostatic pressure assumption clearly leads to an overestimation of the calculated thickness. Even so, away from the areas directly below the escarpment where the difference is bigger, the average shrinking of the GHSF due to the slide event is in the order of only a few meters.

The total volume of sediments that was dropped out of the GHSF due to down-slope mass movement was calculated to be 41.30×10^7 m^3. The volume of sediments that remained undisturbed above the paleo-GHSF base is estimated to be 2.79×10^{10} m^3. With a maximum hydrate occupation of 10% of the pore spaces (Hovland et al., 1997) and assuming an average porosity of 50%, the total volume of dissociated hydrate due to sliding is estimated to be 2.07×10^7 m^3. At the maximum, one volume of gas hydrate yields approximately 0.8 volumes of water and 164 volumes of free gas at STP conditions (Kvenvolden, 1998). Thus, the total amount of destabilising gas hydrates in this area would release 338.66×10^7 m^3 gas and 1.65×10^7 m^3 water at STP conditions. At in situ pressures of about 13–14 MPa, the volume of released gas would not exceed approximately 2.65×10^7 m^3, due to the high compressibility of the (ideal) gas. Thus, at approximate in situ conditions, the initial volume of 2.07×10^7 m^3 of dissociating gas hydrate releases in total about 4.30×10^7 m^3 of gas and water. In other words, an excess fluid volume of approximately 2.2×10^7 m^3 needs to be redistributed in the pore spaces and will create overpressures. The crucial point in estimating the degree of these overpressures and, thus, the possible impact of hydrate decomposition on slope stability, is the time scale of the dissociation process, as the only thing needed for overpressures to dissipate through non-ideal impermeable media is sufficient time.

If one assumes that the sudden pressure decrease due to sliding will immediately dissociate all hydrate present in the zone that was dropped out of the GHSF, the released fluid volume needs to be redistributed together with the present pore fluids into the same pore volume. Hence, the excess fluid volume is 10–11%. In the most probable case when the pore fluids are considered to be mixed (small gas bubbles in pore water) and thus behaving as a single fluid phase, it is reasonable to assume that the pore pressure will also increase with approximately 10%.

However, in situ hydrate dissociation is most likely to be a slow process, and cannot be compared with the situation of hydrate decomposition during (ODP) core recovery in which the core is submitted to severe pressure reduction combined with significant temperature increase. Immediate and complete hydrate dissociation will not happen due to the sudden depressurisation caused by the slide for the

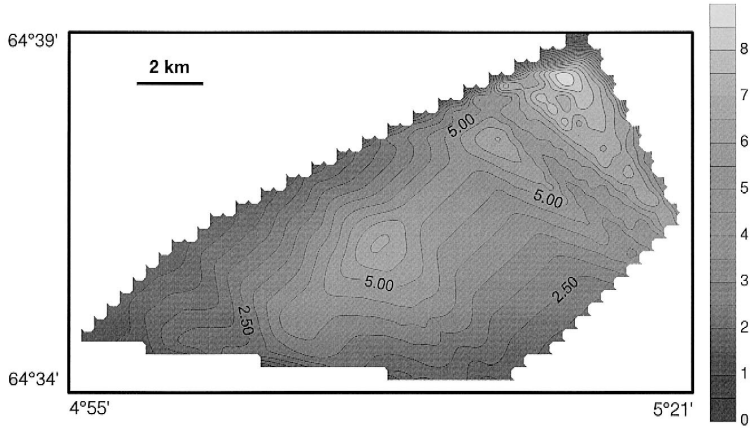


Fig. 15. The calculated thickness of the initially gas-hydrated layer which could fall out of the GHSF due to sliding within the area where the ''lower-slope BSR'' was observed below the slide deposits. Lithostatic pore pressure distribution was assumed.

following reasons. Since the pressure decrease is (nearly) instantaneous and hence much faster than heat exchange mechanisms, this process can be considered as isenthalpic depressurisation. This depressurisation will lead to a temperature drop of the gas and hydrate surface, or more specificly, it will enhance (!) the stability conditions (Sloan, 1998; pp. 549–552). From that moment, conductive heat flow from the surroundings into the hydrates is required to increase the system's temperature and will initiate hydrate dissociation. This process is limited by the rate of heat transfer, depending upon the temperature difference between the hydrate and the surrounding as well as upon geothermal properties of hydrate, host sediments and pore fluids. The partial dissociation of hydrates will then lead to a gradual pore pressure elevation. As this takes place, the heat of hydrate dissociation will be still drawn from the hydrate phase and the surrounding media, preventing the temperature from a fast increase. Thus, this gradual pressure increase at a first approximation can be considered as nearly isothermal and will shift the system back into the conditions favourable for hydrate stability. Continuous heat flow, however, now causes further dissociation, so again the pressure increases and the process starts all over again.

Quantitative estimates of this process are not available yet and additional research is necessary but it is clear that this circular process is not instantaneous at all. Moreover, in less permeable sediments, the hydrate will apparently dissociate slower than in more permeable strata because the excess pore pressure caused by partial dissociation will be dissipated slower and the system will return to hydrate stability conditions much easier.

From the above speculation about the time-scale of the in situ hydrate dissociation due to sliding, it seems to be more reasonable and correct to consider the excess fluid volume to be distributed throughout the entire section of undisturbed sediments above the inferred paleo-BSR, rather than to stay only within the pore space of the initial hydrate-containing sediments. Then, the calculated volume increase (and accordingly the pressure increase) equals only 0.2%, which — in our opinion — can hardly contribute to further regional slope instability.

Even if this is not exactly the case and the time-scale of the hydrate dissociation is, to a certain degree, overestimated, in our simplified calculations we disregarded a number of factors leading to further reduction of resulting overpressures. First, the excess pore pressure is the driving force for internal 3D fluid migration (Darcy's law). Thus, beside vertical fluid displacement, lateral migration will take place as well and the excess volume of fluids will be distributed through a larger pore space than in case when only vertical fluid migration is considered. Moreover, some volume of the migrating fluids can be exhausted through time towards the seafloor, which will also cause a release of excess pore pressure. We also ignored the volume decrease caused by the temperature difference between standard temperature (20°C) and in situ hydrate equilibrium temperature, typically around 10–15°C. Possible partial dissolution of the released gas in the released water was also disregarded. Probably more important, the change of porosity with subbottom depth is ignored as well, while the porous medium is supposed to be homogeneous. All these factors, reducing potential overpressures caused by possible in situ hydrate dissociation due to sliding, allows — in our opinion — for considering at least the order of the obtained estimation as quite reliable.

Of course, these estimates exclude by no means more complicated mechanisms or models in which the dissociation of gas hydrate effectively affects the slope stability. For instance, liquefaction or the release of active fresh water into the clayey environment of glacial/interglacial sedimentary sequence can stimulate formation of so-called ''fast clays'', leading to sediment failure. However, at least the most straightforward and simple mechanism of sliding vs. hydrate-dissociation interrelation will most likely not be considered seriously in this region. In fact, the independence of the observation of the ''lower-slope BSR'' on whether there was sliding above it or not, is itself an indirect evidence of minor, if any, relevance of the sliding to gas hydrate dissociation and vice versa.

6. Conclusions

At the edge of the Vøring Plateau near the Storegga Slide, a distinct BSR forming two laterally

separate zones was observed. The presence of shallow gas accumulations in between of these zones argues for a coupled hydrate formation mechanism in which directional gas migration plays a central role.

The ''lower-slope BSR'' is elongated virtually parallel to the general trend of the slope and is present both below the undisturbed sediments of the plateau, and below the slide scar area and slide deposits. No evidence for fluid venting through the seafloor above the BSRs is observed, except perhaps the slide scarp itself and chaotic seafloor morphology. This ''lower-slope BSR'' is characterised by clear crosscutting of the local stratigraphy and inverse polarity relative to the seafloor reflection.

The ''upper-slope BSR'' fits the area of inferred clay diapirs and is accompanied by numerous fluid escape features on the seafloor (e.g., pockmarks). The ''upper-slope BSR'' also shows reversed polarity, but no clear crosscutting is observed, due to a sedimentation pattern that also parallels the seafloor. However, its acoustic signature and subbottom position is strikingly similar to the situation in the ''lower-slope BSR'' zone. Furthermore, seismic inversion shows a significant relative velocity drop at the BSR interface. Combination of these observations and results allow us to label this reflector as a gas hydrate related BSR.

Over most of the area, the ''lower-slope BSR'' zone is connected to the ''upper-slope BSR'' zone through the presence of enhanced reflectors observed on the acoustic records in the hydrate free zone. These high-amplitude reflectors are found below the theoretical GHSF and are interpreted as indirect evidence of shallow gas accumulations.

Geothermal calculations, based on the BSR subbottom depth and the theoretical three-phase methane — seawater — hydrate equilibrium curve, suggest that the temperature gradient does not vary significantly within the area. Depending on the assumed pore pressure distribution, the geothermal gradient is calculated to be 0.051°C/m (hydrostatic pore pressure) or 0.056°C/m (lithostatic pore pressure).

A model is proposed in which active vertical percolation of gas is present within the zone of ''lower-slope BSR''. Due to the presence of vertical permeability barriers, gas migrates laterally from this region to the area of the diapirs that, in turn, provide pathways for further upward gas migration to the GHSF.

The velocity of vertical fluid migration in the ''lower-slope BSR'' zone was estimated to be at least the order of magnitude of several centimetres per year.

An estimate of possible effect of sliding or earthquake agitation of sediment on gas hydrate destabilisation, which then could facilitate further sediment failure in the area, demonstrates negative results. However, more complicated mechanisms for gas hydrate contribution to slope instability within the area (e.g., formation of ''fast clays'' due to release of active fresh water) cannot be excluded.

Acknowledgements

The authors would like to acknowledge the Scientific Party of the TTR-8 Cruise for fruitful cooperation and stimulating discussions. Personal thanks are addressed to M. Ivanov of UNESCO-MSU Centre for Marine Geosciences for his kind supervision, without which the major part of this work never could have been done. We thank our colleagues from UNESCO-MSU Centre for Marine Geosciences and Renard Centre of Marine Geology, University of Gent. G. Spence and M. Hovland are acknowledged for thoughtful comments and suggestions that undoubtedly improved the manuscript. Our collaboration has been partially supported through the Flemish Government grant RUS.97.05. M. Vanneste is funded by a Ph.D.-grant of the Flemish IWT (Brussels). We are grateful to the captain and the crew of the R.V. Professor Logachev and the technical and administrative staff of the Polar Marine Geosurvey Expedition. We acknowledge the Intergovernmental Oceanographic Commission of UNESCO, Ministry of Science and Technical Policy of the Russian Federation and all other institutes and bodies that supported the TTR-8 expedition. Guinness Breweries, Ireland are acknowledged for the excellent quality of their refreshing beverages, which were really good for us.

Appendix A. Nomenclature, parameters and formulas

A.1. Nomenclature

Symbol	Variables and constant values	Value	Unit
T	Methane–seawater–hydrate equilibrium temperature	–	°C
ρ_{bulk}	Average sediment bulk density	1800	kg m^{-3}
ρ_{sw}	Average sea water density	1025	kg m^{-3}
z	Subbottom depth	–	m
z_{BSR}	Subbottom depth of BSR	–	m
H	Water depth	–	m
$\bar{v}_p$	Mean compressional wave velocity	–	m s^{-1}
v_p	Instantaneous compressional wave velocity	–	m s^{-1}
g	Gravity acceleration	9.81	m s^{-2}
P_{atm}	Atmospheric pressure	0.101325	MPa
P	Methane–seawater–hydrate equilibrium pressure	–	MPa
P_{hydro}	Hydrostatic pressure	–	MPa
P_{lith}	Lithostatic pressure	–	MPa
t_{oneway}	Subbottom one-way travel time	–	s
t_{twoway}	Subbottom two-way travel time	–	s

A.2. Formulas

The formulas mentioned here were used to determine the geothermal field based on the presence of a BSR on the seismic profiles. Once the geothermal gradient is derived, this information is used with the same formulas for the subbottom velocity profiles and the phase boundary to calculate the vertical shrinking of the GHSF due to the sudden lithostatic pressure decrease caused by the slide event, i.e., the situation and result shown in Figs. 14 and 15.

A.2.1. Methane–seawater–hydrate equilibrium curve (Fig. 16)

$$\log P = a + bT + cT^2$$

hence:

$$T = \frac{-b + \sqrt{b^2 + 4c(\log P - a)}}{2c}$$

$a = 0.4684$ $b = 0.0401$ $c = 0.0005$

The constants a, b, c are derived after applying the method of least squares on experimental equilibrium values obtained by Dickens and Quinby-Hunt (1994). Pressure is expressed in MPa, while temperature is expressed in °C. The equation above is valid for the temperature interval $[-2, 15°C]$. The regression coefficient R^2 of this equation is 0.9994.

A.2.2. Pressure distribution

Hydrostatic pressure distribution (MPa):

$$P_{hydro} = P_{atm} + \rho_{sw}\, g(H + z) \times 10^{-6}$$

Lithostatic pressure distribution (MPa):

$$P_{lith} = P_{atm} + g[\,\rho_{sw} H + \rho_{bulk}\, z\,] \times 10^{-6}$$

In this simplified formula, the bulk density is assumed to be constant in the GHSF, so no porosity

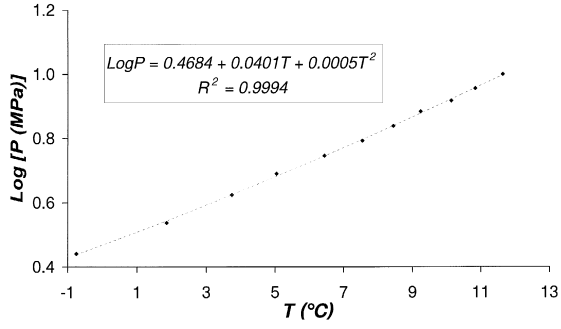


Fig. 16. Pure methane–seawater–hydrate phase boundary and equation, based on experimental data by Dickens and Quinby-Hunt (1994).

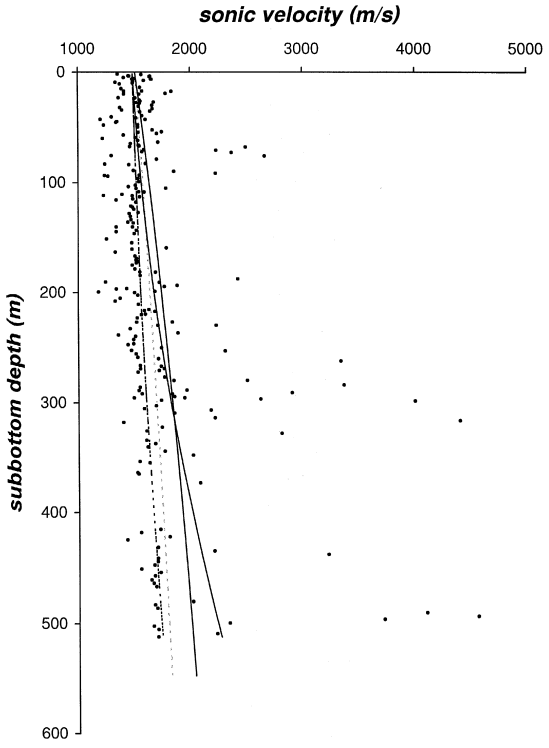


Fig. 17. Subbottom velocity profiles. The dots are measured p-wave velocities from ODP 104, site 642–643 (Eldholm et al., 1987b). The black curves represent instantaneous velocity (solid) and average velocity (dashed). The grey curves are the equivalent Hamilton's regression function (Hamilton, 1980).

changes or compaction effect is taken into account. The maximum average bulk density used, is based upon results from ODP Leg104, site 644 (Eldholm et al., 1987b).

A.2.3. Regression equations (Fig. 17)

Hamilton's equation: Mean and instantaneous compressional wave velocity (m/s) as a function of the subbottom travel time (s) for terrigeneous sediments (silt clays, turbidites, mudstone, shale) (Hamilton, 1980):

$$\bar{v}_p = 1511 + 1041 t_{oneway} - 372 t_{oneway}^2$$
$$= 1511 + 521 t_{oneway} - 93 t_{twoway}^2$$
$$v_p = 1511 + 1983 t_{oneway} - 758 t_{oneway}^2$$
$$= 1511 + 991.5 t_{twoway} - 189.5 t_{twoway}^2$$

Hamilton's equation: conversion to subbottom velocity profiles:

$$\bar{v}_p = -0.0001 z^2 + 0.6195 z + 1511$$

$$v_p = -0.0003 z^2 + 1.1063 z + 1511$$

Subbottom velocity profiles, using ODP-Leg104, site 642 and 643 (Eldholm et al., 1987b)

$$\bar{v}_p = 0.005 z^2 + 0.237 z + 1489.7 \quad R^2 = 0.8718$$

$$v_p = -0.0019 z^2 + 0.548 z + 1489.7 \quad R^2 = 0.1643$$

A.2.4. Geothermal gradient, using BSR equilibrium conditions

$$G = \frac{T - T_0}{z_{BSR}}$$

References

Akentieva, E., Shashkin, P., 1998. Technical report: OKEAN and OREtech side-scan sonars and sonograph processing. In: Kenyon, N., Ivanov, M., Akhmetzhanov, A. (Eds.), Cold Water Carbonate Mounds and Sediment Transport on the Northeast Atlantic Margin: Preliminary Results of Geological and Geophysical Investigations During the TTR-7 Cruise of R.V. Professor Logachev, 1997, 11–12.

Baas, J.H., Mienert, J., Schultheiss, P., Evans, D., 1994. Evidence of gas vents and gas hydrates in the storegga slide area (Norwegian Continental Margin). Abstracts, Gas in Marine Sediments. 3rd International Conference, NIOZ, Texel, The Netherlands, September, 1994.

Bolli, H.M., Saunders, J.B., Perch-Nielson, K., 1985. Plankton Stratigraphy. Cambridge Univ. Press.

Bouriak, S., 1998. Seismic manifestations of gas in the Sorokin trough (Black Sea): Analysis of velocity model obtained by inversion of seismic data. Abstracts, TTR7 post cruise meeting, 7–11 February, Gent, Belgium, p. 85.

Bugge, T., Befring, S., Belderson, R.H., Eidvin, T., Jansen, E., Kenyon, N.H., Holtedahl, H., Sejrup, H.P., 1987. A giant three-stage submarine slide off Norway. Geo-Mar. Lett. 7, 191–198.

Bugge, T., Belserson, R.H., Kenyon, N.H., 1988. The Storegga Slide. Philos. Trans. R. Soc. London A 325, 357–388.

Claypool, G., Kaplan, I., 1974. The origin and distribution of methane in marine sediments. In: Kaplan, I. (Ed.), Natural Gases in Marine Sediments. Plenum, New York, 99–139.

Clennell, M.B., Hovland, M., Booth, J., Henry, P., Winters, W.J., 1999. Formation of natural gas hydrates in marine sediments, part 1: conceptual model of gas hydrate growth conditioned by host sediment properties. J. Geophys. Res., in press.

Dickens, G.R., Quinby-Hunt, M.S., 1994. Methane hydrate stability in seawater. Geophys. Res. Lett. 21 (19), 2115–2118.

Dvorkin, J., Nur, A., 1993. Rock physics for characterisation of gas hydrates. In: Howell, D.G. (Ed.), The Future of Energy Gases. US Geological Survey Professional Paper, 1570, 293–298.

Ecker, C., Dvorkin, J., Nur, A., 1998. Sediments with gas hydrates: internal structure from seismic AVO. Geophysics 63 (5), 1659–1669.

Eldholm, O., Thiede, J., Taylor, E., 1987. Evolution of the Norwegian Continental margin: background and objectives. In: Eldholm, O., Thiede, J., Taylor, E., (Eds.), Proceedings of the Ocean Drilling Program. Initial reports, Leg 104, 5–25.

Eldholm, O., Thiede, J., Taylor, E., 1987. Proceedings of the ocean drilling program. Initial reports, Leg 104, Ocean Drilling Program, College Station, TX.

Eldholm, O., Thiede, J., Taylor, E., 1989. The Norwegian Continental Margin: Tectonic, volcanic and paleoenvironmental framework. In: Eldholm, O., Thiede, J., Taylor, E., et al. (Eds.), Proceedings of the Ocean Drilling Program, Scientific Results, Leg 104. Ocean Drilling Program, College Station, TX, 5–28.

Eldholm, O., Thiede, J., Taylor, E. et al., 1989. Proceedings of the Ocean Drilling Program, Scientific Results, Leg 104, Ocean Drilling Program, College Station, TX.

Evans, D., King, E.l., Kenyon, N.H., Brett, C., Wallis, D., 1996. Evidence for long-term instability in the Storegga Slide region off western Norway. Mar. Geol. 130, 281–292.

Ginsburg, G., Soloviev, V., 1997. Methane migration within the submarine gas-hydrate stability zone under deep-water conditions. Mar. Geol. 137, 49–57.

Hamilton, E.L., 1980. Geoacoustic modelling of the seafloor. J. Acoust. Soc. Am. 68 (5), 1313–1340.

Hjelstuen, B.O., Eldholm, O., Skogseid, J., 1997. Vøring Plateau diapir fields and their structural and depositional settings. Mar. Geol. 144, 33–57.

Hovland, M., Gallagher, J., Clennell, M., Lekvam, K., 1997. Gas hydrate and free gas volumes in marine sediments: Example from the Niger Delta front. Mar. Petrol. Geol. 14, 245–255.

Hovland, M., Judd, A.G., 1988. Seabed Pockmarks and Seepages: Impact on Geology, Biology and the Marine Environment. Graham and Trotman, London, p. 293.

Hyndman, R., Davis, E., 1992. A mechanism for the formation of methane hydrate and seafloor bottom-simulating reflectors by vertical fluid expulsion. J. Geophys. Res. 97 (5), 7025–7041.

Hyndman, R., Spence, G., 1992. A seismic study of methane hydrate marine bottom simulating reflectors. J. Geophys. Res. 97 (B5), 6683–6698.

Jansen, E., Befring, S., Bugge, T., Eidvin, T., Holtedahl, H., Sejrup, H.P., 1987. Large submarine slides on the Norwegian continental margin: sediments, transport and timing. Mar. Geol. 78, 77–107.

Kvenvolden, K.A., 1993. Gas hydrates: geological perspective and global change. Rev. Geophys. 31 (2), 173–187.

Kvenvolden, K.A., 1998. A primer on the geological occurrence of gas hydrate. In: Henriet, J.-P., Mienert, J (Eds.), Gas Hydrates: Relevance to World Margin Stability and Climate Change, Geological Society of London, Special Publications, 137, 9-30.

Kvenvolden, K.A., Golan-Bac, M., McDonald, T.J., Pflaum, R.C., Brooks, J.M., 1989. Hydrocarbon gases in sediments of the Vøring Plateu, Norwegian Sea. In: Eldholm, O., Thiede, J., Taylor, E., et al. (Eds.), Proceedings of the Ocean Drilling Program, Scientific Results, Leg 104, Ocean Drilling Program, College Station, TX, 291–307.

Lammers, S., Suess, E., Hovland, M., 1995. A large methane plume east of Bear Island (Barents Sea): implications for the marine methane cycle. Geologische Rundschau 84, 59–66.

Lavergne, M., Willm, C., 1977. Inversion of seismograms and pseudo velocity logs. Geophys. Prospect. 25 (2), 231–250.

Lindseth, R.O., 1979. Synthetic sonic logs — a process for stratigraphic interpretation. Geophysics 44 (1), 3–26.

Mienert, J., Posewang, J., Baumann, M., 1998. Gas hydrates along the north-eastern Atlantic margin: possible hydrate bound margin instabilities and possible release of methane. In: Henriet, J.-P., Mienert, J. (Eds.), Gas Hydrates: Relevance to World Margin Stability and Climatic Change, Geological Society of London, Special Publication, 137, 275–291.

Minshull, T.A., Singh, S.C., Westbrook, G.K., 1994. Seismic velocity structure at a gas hydrate reflector, offshore Western Columbia, from full waveform inversion. J. Geophys. Res. 99 (B3), 4715–4734.

Muller, 1978. Tertiary and Quaternary Calcareous nannoplankton in the Norwegian-Greenland Sea. In: White, S.M. (Ed.), Initial Reports of the Deep Sea Drilling Project, Leg 38, 823-841

Posewang, J., Mienert, J., 1996. Gas hydrates and free gas in sediments of the Norwegian Continental Margin: results from wide-angle seismic experiments. In: Mienert, J., Henriet, J.P. (Eds.), Gas Hydrates: Relevance to World Margins Stability and Climatic Changes, Abstract Book, 70, Gent, 18–22 September.

Rabinowitz, P.D., Baldauf, J.G., Garrison, L.E., Meyer, A.W., 1992. Ocean drilling on passive continental margins. In: Watkins, J.S., Zhiqiang, F., McMillen, K.J., (Eds.), Geology and Geophysics of Continental Margins, American Association of Petroleum Geologists, Chap. 22, 399–414.

Rempel, A., 1995. Theoretical and experimental investigations into the formation and accumulation of gas hydrates. MSc Thesis, University of British California, p. 122.

Rempel, A., Buffett, B., 1998. Mathematical models of gas hydrate accumulation. In: Henriet, J.-P., Mienert, J. (Eds.), Gas Hydrates: Relevance to World Margin Stability and Climate Change, Geological Society of London, Special Publications, 137, 63–74.

Russel, B.H., 1988 Introduction to seismic inversion methods. Society of Exploration Geophysicists, Course Notes Series, 2.

Sloan, E.D., Jr., 1998. Clathrate hydrates of natural gases, 2nd edn., Marcel Dekker, New York, p. 703.

Thiede, J., Eldholm, O., Taylor, E., 1989. Variability of Cenozoic Norwegian-Greenland Sea paleoceanography and northern hemisphere paleoclimate. in: Eldholm, O., Thiede, J., Taylor, E. et al. (Eds.), Proceedings of the Ocean Drilling Program, Scientific Results, Leg 104, Ocean Drilling Program, College Station, TX, 1067–1118.

Yamano, M., Uyeda, S., Aoki, Y., Shipley, T.H., 1982. Estimates of heat flow derived from gas hydrates. Geology 10, 339–342.

Zatsepina, O., Buffett, B., 1998. Thermodynamic conditions for the stability of gas hydrate in the seafloor. J. Geophys. Res. 103 (10), 24127–24139.